Effect of medium-high temperature conditioning on the mechanical properties of single quartz fibres

Ginevra Lalle [a],*, Edoardo Rossi [b], Marco Sebastiani [b], Fabrizio Sarasini [a], Jacopo Tirillò [a]

[a] *Department of Chemical Engineering Materials Environment, Sapienza-Università di Roma, Via Eudossiana 18, 00184 Rome, Italy*
[b] *Engineering Department, Roma Tre University, Via della Vasca Navale 79, 00146 Rome, Italy*

ABSTRACT

This work adopted multi-scale characterizations to investigate the effects of exposure to medium-high temperatures (600–800 °C) on the mechanical properties of single quartz fibres, focusing on whether bulk property changes, i.e., Young's modulus, density and fracture toughness, occur and can be related to the thermal strength loss, herein quantified as 75% up to 86% with increasing temperature. Investigation of the fracture surfaces through scanning electron microscopy revealed that failure originated from the fibre surface regardless of heat treatment. Neither bulk crystallization was highlighted through X-ray diffraction nor relevant changes or gradients of Young's modulus and hardness were disclosed over the fibre cross-sections through high-speed nanoindentation mapping. A 9% increase in fracture toughness measured through micro-pillar splitting revealed a slightly improved crack propagation resistance that cannot compensate for the drastic effect responsible for strength reduction, which is discussed in terms of surface-controlled mechanisms involving the development and growth of surface flaws.

1. Introduction

Quartz fibres (QFs), or ultrapure silica glass fibres (99.99% SiO_2), are excellent reinforcements for high-performance composite materials. With lightweight properties, low dielectric constant and dielectric loss, and good chemical stability, quartz fibres are widely used as reinforcing fibres for wave-transparent composite radomes and antenna windows in aviation, aerospace, and 5 G communication services [1–3]. Compared to common reinforcing fibres such as E-glass, high silica, and basalt fibres, quartz fibres possess superior properties at high temperatures, including low coefficient of thermal expansion, low thermal conductivity, high thermal shock resistance, and ablation resistance, which make them especially suited for heat insulation and shielding functions in aerospace and military aircrafts [1,4,5].

However, despite their high in-service temperature limit (1050–1200 °C) and softening temperature (1710 °C), the use of quartz fibres in high-temperature environments may be hindered by the degradation of the fibre mechanical response following thermal exposure. Amorphous quartz fibres usually undergo devitrification into α-cristobalite in the temperature range 1100–1435 °C [6,7], which produces cracking and degradation of the fibre surface. Furthermore,

their tensile strength has been reported to degrade at temperatures as low as 500 °C [8–10].

The degradation of the fibre mechanical properties after exposure to high temperatures has been previously reported for various fibres, focusing on understanding the controlling mechanisms. The strength of E-glass fibres has been found to drop by 50–70% over the temperature range of 450–600 °C [11–13]. Similarly, basalt fibres undergo a strength loss of around 75% following heat treatments at 600 °C [14], regardless of the higher operating and softening temperatures of basalt fibres (~650 °C and 1050 °C, respectively) compared to E-glass fibres (~460 °C and 600 °C, respectively). Several damage mechanisms, classified as surface and structural phenomena, have been proposed to address the issue of thermal strength degradation of these fibres. The two main surface phenomena are sizing removal [15] and thermally induced diffusion of water [16]. Thermal exposure can also cause structural relaxation of the anisotropic silica network structure originated by the high drawing stress during the fibre fabrication [17,18]. As a consequence, the loss of the mechanical strength of glass and basalt fibres is usually accompanied by increases in the room-temperature density and Young's modulus of heat-treated fibres [12,14,19].

Along with the fibre tensile strength and Young's modulus, a

property which has recently received significant interest in studies of fibres damage modes after thermal exposure is the Mode-I fracture toughness (K_{IC}). By measuring this property, the effect of heat treatment on the strength-flaw relationship can be disclosed. Lilli et al. [20] recently reported an increase in basalt fibres' Mode-I fracture toughness, K_{IC}, after heat treatment (400–600 °C) in air. This revealed the occurrence of structural changes able to influence the strength-flaw relationship for basalt fibres. Moreover, high-speed nanoindentation mapping of the fibre cross-sectional area directly observed local radial heterogeneity, displaying the formation of ordered and compact structures at the fibre skin characterized by higher elastic modulus.

While the thermal degradation of glass and basalt fibres has been widely investigated in the literature, limited research has been conducted on quartz fibres. Only recently, Zheng et al. [21] studied the morphology, surface structure and tensile strength of quartz fibres after 10-hour exposure in the temperature range 600–900 °C in air atmosphere. Based on scanning electron microscopy (SEM), transmission electron microscopy (TEM), X-ray diffraction (XRD), and tensile tests, they revealed the formation of nanometre crystallites on the fibre surface, which are considered to produce new surface defects, leading to strength retention up to only 1/30 of the fibre original mechanical strength after exposure at 900 °C. However, whether the bulk fracture properties of quartz fibres are affected by thermal exposure is not detailed.

In this context, this work aims to contribute to a more thorough understanding of the effects of exposure to medium-high temperatures (600, 700, 800 °C) on the mechanical properties of quartz fibres. The variations of tensile strength, Young's modulus, Weibull parameters, density, surface morphology and microstructure are provided as a function of heat-treatment temperature. Moreover, the evolution of quartz fibre fracture toughness is assessed by an innovative nanoindentation-based technique, namely the pillar splitting method, recently introduced and optimized by Sebastiani et al. [22–25]. Traditionally, the estimation of K_{IC} has involved considerable uncertainties and complexity, as it required the determination of the initial flaw size from the fibre fracture surface or the introduction of an artificial notch of known size and shape in the fibre plane with a focussed ion beam (FIB), causing FIB damage and residual stresses which can affect the measured K_{IC}. Both mentioned issues are solved in the pillar splitting method as it does not require the crack length to be measured and the residual stresses are released during the pillar fabrication by FIB milling. In addition, this work adopted high-speed nanoindentation mapping to disclose possible heterogeneities of Young's modulus and hardness over the cross-sections of as-received and heat-treated fibres.

The outcomes of this study point towards a damage mechanism that is mainly active at the fibre surface. No bulk crystallization phenomena or significant changes in the bulk properties were detected except for a slight increase in the fracture toughness from the non-treated to the 800 °C treated fibres, which highlights a modification in the crack propagation resistance following heat treatment.

2. Materials and methods

2.1. Raw materials

Quartz fibres were supplied by Saint-Gobain as a continuous roving with a nominal fibre diameter of 14 μm, linear density of 1600 tex, and sized with a commercial epoxy resin compatible sizing (Quartzel® C14 1600 QS1318).

2.2. Fibre heat treatment

Bundles of as-received quartz fibres were heat treated using a tube furnace (Lenton Thermal Designs Ltd., Hope, UK). Temperatures of 600, 700, and 800 °C were selected to investigate quartz fibre strength loss with increasing temperature. Each thermal treatment was carried out in

air for 1 h. Finally, the fibres were removed from the furnace and cooled at room temperature.

2.3. Single fibre tensile testing

Tensile tests on as-received and thermally treated quartz fibres were performed utilizing a Zwick/Roell Z010 tensile machine equipped with a 100 N range load cell. Tests were performed at room temperature, in displacement control, and with a 2 mm/min cross-head speed. Individual filaments, carefully separated by hand from the fibre bundles, were glued onto a card tab with a central cut-out window equal to the gauge length. Three different gauge lengths were selected for as-received quartz fibres, namely 20 mm, 30 mm, and 40 mm, while heat-treated fibre samples had a gauge length of 20 mm. At least 20 samples were tested for each gauge length and heat-treatment temperature. The average fibre diameter was evaluated using an optical microscope Nikon Eclipse 150 L equipped with Lucia Measurement image analysis software. The displacement associated with the system compliance was subtracted from the total cross-head displacement to determine the actual fibre elongation in the gauge length. The system compliance was calculated according to ASTM C1557 [26] by obtaining the force versus displacement behaviour of the fibres at the three selected gauge lengths.

The dispersion of the tensile strength and Young's modulus values was statistically analysed using a two-parameter Weibull distribution, according to Eq. (1):

$$F(\sigma) = 1 - \exp\left[-\left(\frac{\sigma}{\sigma_0}\right)^m\right] \tag{1}$$

where $F(\sigma)$ is the cumulative probability of failure at the applied stress σ, m is the Weibull modulus and σ_0 is a scale parameter. The parameters of the Weibull distribution for each set of tested fibres, i.e., m and σ_0, were estimated through the maximum likelihood estimation method (MLE). In addition, 90% confidence intervals (CI) and the unbiased estimates of Weibull moduli, m_u, were calculated according to the standard ISO 20501:2019. The estimator in Eq. (2) was used for the probability of failure in the graphical representation of ln{ln[1/(1-F)]} against ln(σ):

$$F_j = \frac{j - 0.5}{N} \tag{2}$$

where N is the number of tested fibres and j is the rank of the jth data point [27].

2.4. Thermogravimetric analysis (TGA)

The mass loss of as-received quartz fibres with temperature was analysed through a SetSys Evolution (Setaram Instrumentation) thermogravimetric analyser. The fibres were heated up to 800 °C at 10 °C/min in a nitrogen atmosphere.

2.5. Density measurement

Helium pycnometry (AccuPyc II 1340) was employed to measure the density of both as-received and heat-treated quartz fibres and evaluate possible variations of the fibre density following thermal exposure.

2.6. X-ray diffraction (XRD) analysis

As quartz fibres are fully amorphous in nature, crystallization phenomena may occur after exposure to high temperatures. Therefore, X-ray diffraction (XRD) analysis was performed on as-received and heat-treated quartz fibres to assess the effects of thermal exposure on the fibre structure. The study was carried out at room temperature on a Philips X'Pert PRO powder diffractometer (Cu$_{K1}$ α radiation = 1.54060 Å, Cu$_{K2}$ α radiation = 1.54443 Å). XRD patterns were collected in the range of 2θ = 10°-70° with a scan step 2θ = 0.02° and scan rate of

1°/min.

2.7. Scanning electron microscopy (SEM)

The lateral surfaces of as-received and heat-treated quartz fibres were examined using a Mira3 field emission scanning electron microscope by Tescan. Furthermore, after tensile testing, the fracture surfaces of the fibres were observed to highlight the effect of temperature on the fracture mechanism. The samples were sputter coated with gold prior to investigation.

2.8. High-speed nanoindentation mapping

High-speed nanoindentation mapping [28,29] was performed for high-throughput mapping of mechanical properties and identification of local heterogeneities distribution over the polished cross-section of as-received and heat-treated quartz fibres. To ensure a structurally stable alignment of the single fibre with the nanoindentation instrument testing axis, fibre bundles were embedded in an epoxy matrix, ensuring accurate planar positioning of their cross-sectional area to the mounted free surface. Experiments were conducted using a G200 nanoindenter (KLA Corporation, Oak Ridge, TN, USA) with a standard Berkovich tip. High-speed grid indentations with lateral extensions of $20 \times 20 \mu m$ were realized, centred on each fibre. At least three fibres were examined for each sample. The target load for testing was extracted by previously acquired load-indentation depth relationships from Continuous Stiffness Measurement (CSM) data quasi-static nanoindentation, allowing achievement of an average indentation depth on the ceramic fibre of ~80 nm. The accurate positioning for each indent at 1/5th of the reached indentation depth, as allowed for ceramic materials [30,31], was ensured by a nano-positioning NanoVision stage (Physik Instrumente (PI) GmbH & Co.), allowing for 500 nm laterally resolved maps with a total number of indents, on average, of 1936. The machine compliance and indenter area function were calibrated with varied loads on a certified Fused Quartz reference sample, before and after each specimen testing.

After performing the experiments, data filtering of hardness and elastic modulus 2D maps was applied to exclude contributions of the polymeric matrix to the determination of local heterogeneities in the fibre. Statistical deconvolution algorithms based on probability distribution function (PDF) and k-means clustering were used to evaluate property variations within the fibre, according to well-established procedures [30,32,33].

2.9. Fracture toughness measurements via pillar-splitting

The micro-scale fracture toughness of single quartz fibres was evaluated through the pillar splitting method [22–25], which employs focused ion beam (FIB) micro-milling to produce pillars that are loaded till rupture during subsequent sharp nanoindentation testing. The fracture toughness is easily calculated through the following Eq. (1) by measuring the pop-in (failure) load:

$$K_c = \gamma \frac{P_c}{R^{3/2}} \tag{3}$$

Where K_c is the fracture toughness (MPa•$\sqrt{m}$), P_c is the critical load for unstable pillar failure, R is the measured pillar radius (μm), and γ is a dimensionless coefficient calculated by Finite Element Modelling (FEM). A previous work [34] has presented the variation of such coefficient for a wide range of material properties (H/E ratio and Poisson's ratio), as well as for a range of sharp indenter angles (including the most used Berkovich and Cube-Corner indenters). The γ coefficient was extracted from high-speed mapping values averaging elastic modulus and hardness within the relevant corresponding areas to the position of the FIB milled pillars.

In this work, pillars having a diameter (D) of 4.06 μm and an aspect ratio $h/D \geq 1$ were fabricated, using a Helios Nanolab 600 FIB/SEM microscope (ThermoFisher Scientific) at the centre of defect-free single fibres. A multi-step semi-automated FIB milling procedure was adopted, involving a coarse milling phase with a current of 0.46 nA and a final multi-step polishing and edge sharpening phase at 28 pA (Fig. 1a) to minimize FIB artefacts. The ion beam voltage was 30 kV. Some pillars were FIB-sectioned after fabrication (Fig. 1b) to accurately measure the diameter and taper angle and investigate the presence of pre-existing cracks in the sample material.

Pillar splitting tests were performed using a Keysight G200 nano-indenter equipped with a Cube-Corner indenter. Calibration was carried out on a Fused Quartz reference sample, according to the standard ISO 14577–1–2–3. Experiments were performed using a constant strain rate of 0.05 s^{-1}, until unstable failure of the pillar was achieved (as identified by a pop-in event in the load-displacement curve). Results from at least five pillars contributed to determining the fracture toughness at the fibre centre. It is worth mentioning that residual imprints and cracks in the fibre, as shown in Fig. 1d, correspond to events occurring after the splitting of the central pillar and are due to abrupt precipitation of the indenter towards the substrate after the pop-in event.

Additionally, 3 μm diameter pillars, following the same fabrication principles, have been realized on single fibre peripheral areas to investigate toughness dependence upon diametral positioning (Fig. 1c).

3. Results and discussion

3.1. Mechanical characterization of untreated and heat-treated quartz fibres

To assess the effects of high-temperature exposure on the mechanical properties of quartz fibres, the tensile properties of as-received fibres were first evaluated at three different gauge lengths, namely 20 mm, 30 mm, and 40 mm. Subsequently, quartz fibres were heat treated at 600 °C, 700 °C and 800 °C for 1 h in air atmosphere, and further tensile tests were performed on the heat-treated fibres, maintaining a constant gauge length of 20 mm. The results from the tensile tests and the values of the characteristic parameters of the Weibull distribution are reported in Tables 1 and 2, respectively.

The measured tensile strengths and strains at failure were found to depend on the gauge length, as typically observed for ceramic fibres [14, 15,35]. In fact, the tensile strength of brittle materials exhibits a dimension effect, being higher at shorter gauge lengths and decreasing with an increase in the fibre length. The same is true for strains at failure, while Young's modulus showed no clear dependence on the gauge length, as supported by previous works on ceramic fibres [14,15,35]. A decreasing trend of the mechanical strength was detected with increasing heat-treatment temperature. The heat treatment at 600 °C caused the fibre strength to drop by approximately 74%. This finding reveals that, despite the higher in-service and softening temperatures, high-purity quartz fibres undergo a mechanical strength loss comparable to that of general-purpose glass fibres and basalt fibres up to 600 °C [11–14,36,37]. A strength degradation of 76% was detected for quartz fibres heat-treated at 700 °C, while an even more severe strength drop was caused by the exposure at 800 °C, which resulted in a strength loss of approximately 86%.

The measured strength losses compare quite favourably with those from previous studies [8–10,21,38], highlighting that high-temperature exposure can seriously compromise the mechanical response of quartz fibres and make further investigation necessary on both untreated and heat-treated fibres to identify the possible damage mechanisms. Weibull plots of tensile strength and Young's modulus (Fig. 2) indicate that a unimodal Weibull function well describes the tensile test data, as the values are arranged according to a linear trend. This suggests the existence of a single-flaw population responsible for the failure of quartz fibres. Moreover, as a linear trend was obtained for both as-received and
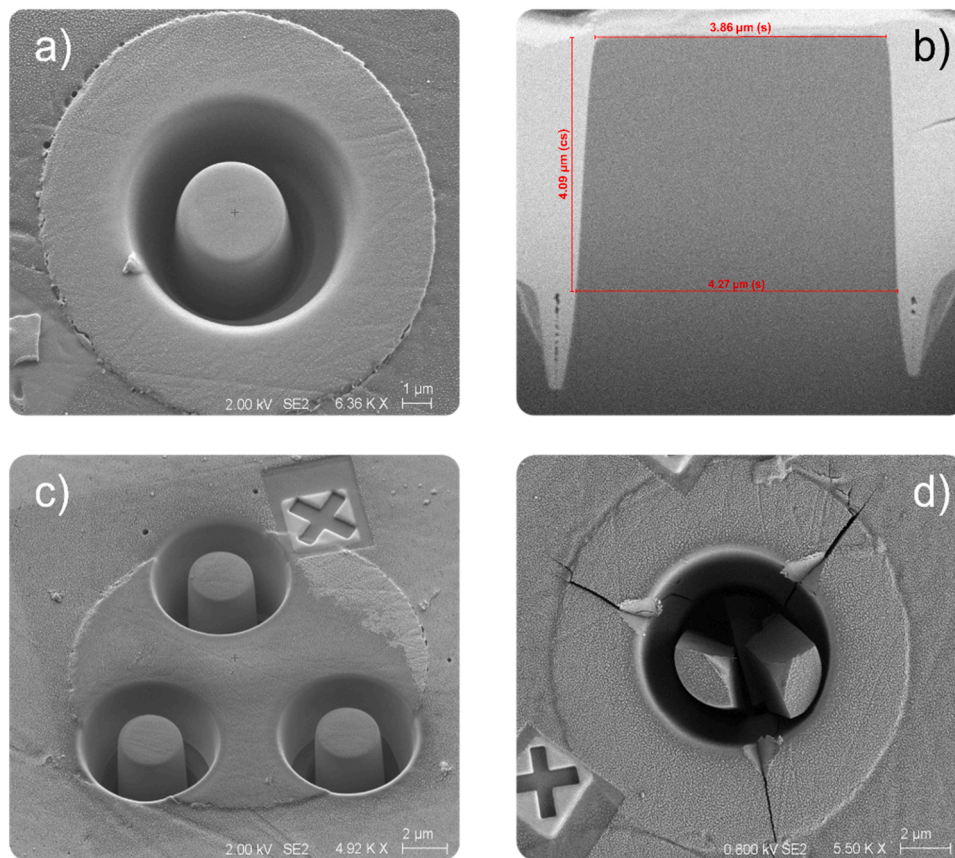
Fig. 1. The micro-pillar splitting methodology involved a) fabrication of 4 μm diameter pillars at each fibre centre using a standardized procedure for reproducibility and b) FIB cross-sectioning to assess the shape and tapering angle. c) Carousel of micro-pillars having 3 μm diameter at fibres edge to highlight gradients from edge to centre of fracture toughness. d) Representative post-mortem image of a micro-pillar.

Table 1
Results of tensile tests for as-received (R.T.) and heat-treated single quartz fibres in terms of average values (average value/standard deviation).

Heat-treatment temperature (°C)	Gauge length (mm)	Diameter (μm)	Tensile strength (MPa)	Young's modulus (GPa)	Strain at failure (%)
R.T.	20	14.3/0.3	1974.5/364.4	75.5/3.1	2.6/0.5
R.T.	30	14.6/0.4	1277.0/293.0	67.2/3.6	1.9/0.5
R.T.	40	14.6/0.4	1136.0/275.4	74.1/3.4	1.5/0.4
600	20	14.7/0.4	506.4/118.6	71.7/3.8	0.7/0.2
700	20	14.5/0.7	464.5/118.4	66.5/3.4	0.7/0.2
800	20	14.0/0.4	274.3/74.7	73.4/3.9	0.4/0.1

heat-treated fibres (Fig. 3), it can be assumed that high-temperature exposure does not involve a change in the nature of defects but rather in their severity and homogeneity, which can be qualitatively described by the detected variations of the Weibull parameters (Table 2) [39,40]. As already observed for the mean values, a decreasing trend can be clearly identified for the values of the characteristic strength, revealing that the average size of critical defects was increased by heat treatment. On the other hand, the similar values of $m_{\sigma,u}$ and the highly overlapping confidence intervals indicate no significant difference in shape parameter between the distributions, suggesting that the same flaw types were active in all specimen sets.

To determine the nature and the location of the critical fracture origin, the cross-section of the fracture surfaces after tensile tests was analysed by scanning electron microscopy, revealing a characteristic morphology typical of the fracture mechanism of brittle materials (Fig. 4) [20,41,42]. As the fracture occurred, changes in the crack propagation rate originated three different regions, namely mirror, mist, and hackle, irrespective of heat-treatment temperature. The location of the mirror zone, highlighted with a white dashed line, indicates that the fracture initiated from the fibre surface, thus revealing that superficial flaws are responsible for fibre breakage. Heat treatment was found to affect only the size of the mirror zone, which increased with an increase in the heat-treatment temperature and can be correlated with strength loss [37]. No signs of visible flaws were detected at the fracture origin. While it is possible that the sputtered gold coating – even if very thin – may have obscured such features, the difficulty of characterizing the fracture-triggering flaw on the fibre fracture surfaces is also to be considered, with no flaws observed at the origin for the majority of the mirror regions examined in literature [43,44].

It is worth noting that possible superposition of a certain amount of bending onto the tensile loading may be produced by inaccuracies in the alignment between the fibre and the loading direction. While the effect of the misalignment on the value of the tensile strength can be neglected at the gauge lengths used in the present work [45], a certain amount of bending can enhance the predominant failure from the surface and mask the failure from the volume defects. Nevertheless, the failure of brittle fibres, such as glass and basalt fibres, is often reported to be governed by surface flaw distributions [11,14,20,37], making it reasonable to assume it also valid for quartz fibres.

SEM micrographs (Fig. 5) revealed that the lateral surface of as-received quartz fibres is smooth, while some irregularities arise after heat treatment. The homogeneous surface observed in the case of as-

Table 2

Weibull distribution parameters estimated through MLE for as-received (R.T.) and heat-treated single quartz fibres. Confidence intervals (CI) at 90% and the unbiased estimate of the shape parameters ($m_{\sigma,u}$, $m_{E,u}$) are provided for both tensile strength and Young's modulus.

| Heat-treatment temperature (°C)	Gauge length (mm)	Tensile strength - m_σ [90% CI]	Tensile strength – $m_{\sigma,u}$	Tensile strength – σ_0 [90% CI] (MPa)	Young's modulus – m_E [90% CI]	Young's modulus – $m_{E,u}$	Young's modulus – E_0 [90% CI] (GPa)
R.T.	20	6.2 [4.3, 7.8]	5.8	2125.3 [1989.0, 2273.3]	29.9 [20.9, 37.6]	27.9	77.0 [75.9, 78.0]
R.T.	30	5.0 [3.6, 6.3]	4.7	1391.1 [1287.6, 1504.6]	20.6 [14.7, 25.7]	19.4	68.9 [67.6, 70.2]
R.T.	40	4.9 [3.0, 5.8]	4.1	1243.8 [1121.8, 1381.5]	24.9 [16.5, 32.0]	22.9	75.6 [74.2, 77.1]
600	20	5.1 [3.8, 6.1]	4.8	552.7 [519.0, 588.9]	17.5 [13.3, 21.1]	21.1	73.6 [72.2, 74.9]
700	20	4.4 [3.4, 5.4]	4.3	510.0 [475.4, 547.6]	21.0 [16.1, 25.4]	20.2	68.1 [67.1, 69.1]
800	20	4.3 [3.0, 5.5]	4.0	302.1 [273.4, 334.4]	17.9 [12.2, 22.8]	16.6	75.3 [73.5, 77.1]
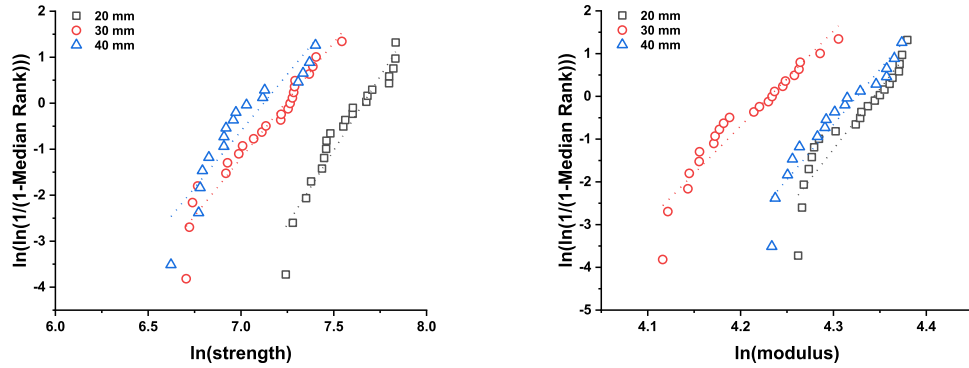
Fig. 2. Weibull plots of (left) the tensile strength and (right) Young's modulus of single quartz fibres as a function of gauge length.
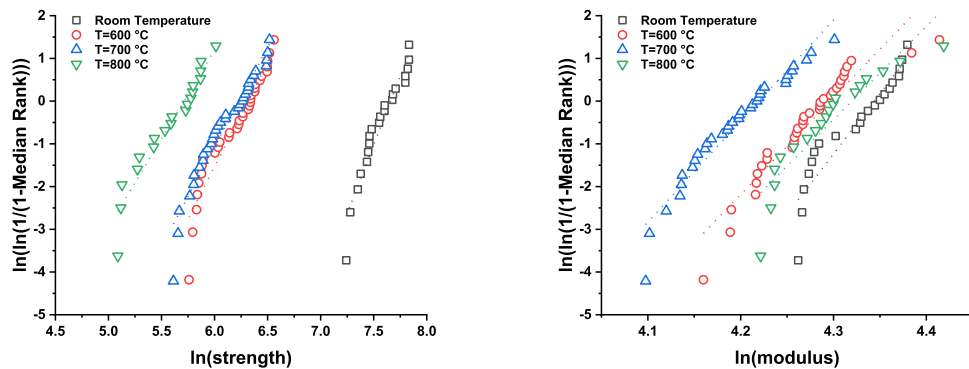

Fig. 3. Weibull plots of (left) the tensile strength and (right) Young's modulus of single quartz fibres as a function of heat-treatment temperature.
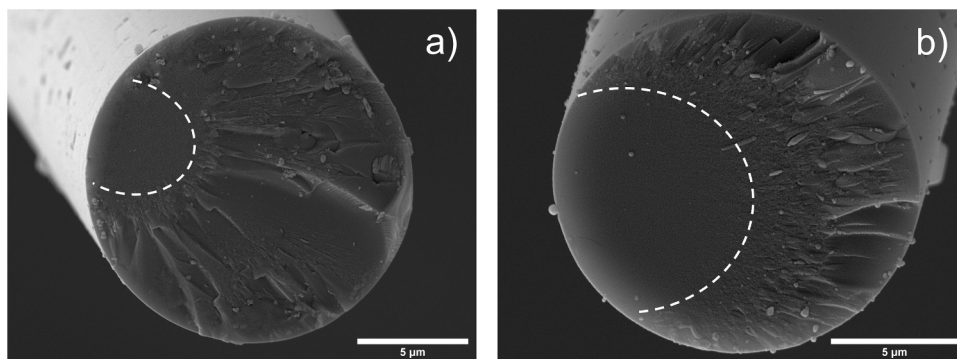

Fig. 4. SEM micrographs of the fracture surfaces of (a) untreated quartz fibres and (b) heat-treated quartz fibres at 800 °C. The mirror zone is highlighted with a white dashed line.
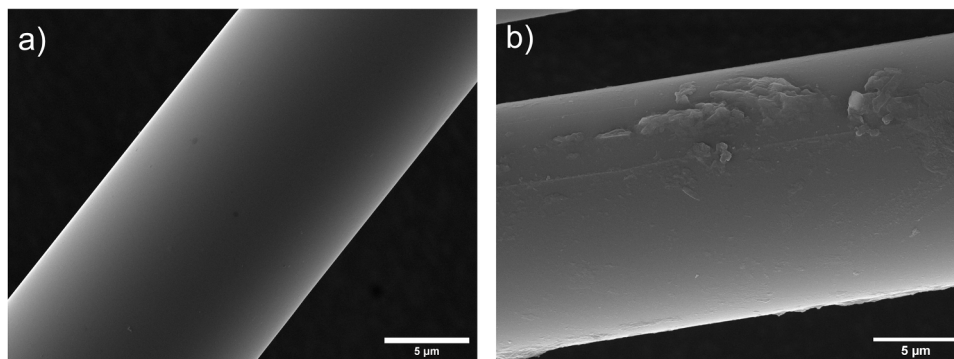
Fig. 5. SEM micrographs detailing the lateral surface of (a) untreated and (b) heat-treated (800 °C) quartz fibres.

received quartz fibres can be ascribed to commercial epoxy resin-compatible sizing. As recently demonstrated by Thomason [46], epoxy-compatible glass fibre sizings degrade relatively rapidly above 250 °C, often reaching complete degradation at temperatures as low as 500 °C [37,46]. Thermogravimetric analysis (Fig. 6) performed on as-received quartz fibres confirmed the occurrence of sizing degradation, with a total weight loss at 800 °C amounting to less than 0.1% of the initial weight. Sizing degradation occurred in the temperature range of 150–550 °C, with a maximum degradation rate at 330 °C, as shown by the DTG curve. Based on these findings, it can be concluded that heat treatments led to the loss of protective sizing, thus determining the exposure of inherent fibre flaws. According to Zinck [39], a flaw-healing effect is observed when fibres are coated with an organic sizing, leading to higher mechanical strength. Sizing removal can therefore be identified as one of the main factors determining quartz fibre strength loss, as usually reported for glass fibres [12,36]. Moreover, removing protective sizing exposed the fibres to mechanical handling damage, which is at play during the removal of single fibres from heat-treated bundles. However, it is worth noting that the exposure of the inherent flaws and mechanical handling damage due to sizing degradation should affect the strength of all heat-treated fibres to the same extent, suggesting the existence of fundamental thermal effects responsible for the further strength losses detected with increasing temperature.

Amorphous quartz fibres are prone to crystallization when exposed to high temperatures [17]. The devitrification process has been previously reported as the main cause of quartz fibre thermal degradation, as it can produce volume changes that compromise the original structural integrity of the fibres, thus having a tremendous impact on the fibre mechanical properties [7]. The crystallization of quartz fibres occurs at lower temperatures (1100–1435 °C) than bulk quartz glass, due to the

small diameter and high surface energy of quartz fibres which promote the surface nucleation of crystals. It is noteworthy that Zheng et al. [21] recently observed the formation of nanometre-ordered regions localized at the fibre surface after exposure at temperatures as low as 700 °C and the nucleation of surface nanometre crystallites at 900 °C. In this study, diffraction analysis (Fig. 7) revealed that quartz fibres exhibited an amorphous structure up to 800 °C. The possibility of surface crystallization has not been directly investigated, as it cannot be easily identified with the XRD method, but it is consistent with the obtained results. In fact, besides excluding the occurrence of bulk crystallization phenomena, the obtained XRD spectra strengthen the hypothesis of a failure mechanism that occurs predominantly at the surface, with no structural ordering processes taking place in the bulk of the fibre.

Indirect evidence of this is provided by the measured Young's modulus which, unlike tensile strength, was hardly affected by thermal exposure, implying no bulk modification phenomena being involved, as supported by a previous work on quartz fibres [38]. On the contrary, an increase in stiffness with increasing temperature has been commonly reported for general-purpose glass fibres and basalt fibres [12,14,18–20] due to a thermally-induced structural relaxation phenomenon occurring in the bulk of the fibre. Consequently, the density of glass and basalt fibres increased due to heat-treatment temperature. Regarding quartz fibres, Table 3 shows no significant variations in the measured fibre density, confirming that no relevant bulk modification occurred.

To address the complex issue of the thermal degradation of quartz fibres, the thermal and mechanical history of the fibre should also be considered. During manufacture, the drawing stresses and the high cooling rate are believed to produce structural anisotropy and excess enthalpy due to changes in the Si-O-Si bonding angles and the silica network structure deformation, respectively. These phenomena have previously been used to explain the superior strength of glass fibres compared to bulk glass. On the other hand, high-temperature exposure
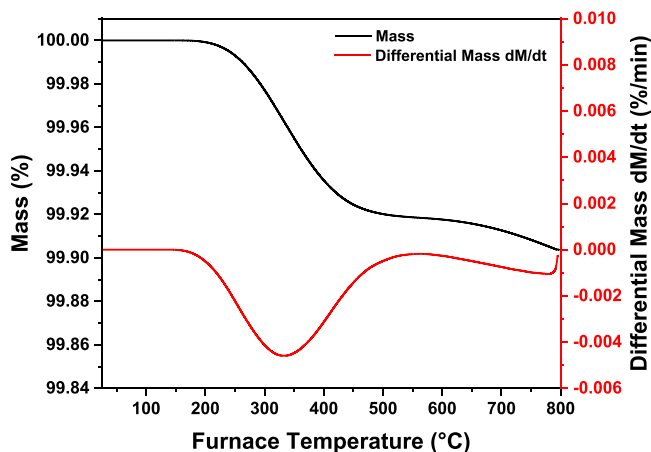

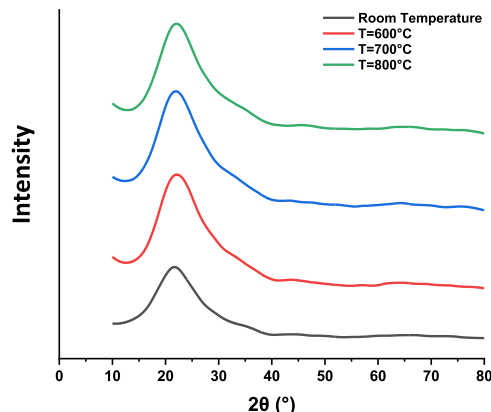**Fig. 6.** TGA and DTG curves from thermogravimetric analysis performed on as-received quartz fibres.

Fig. 7. X-ray diffraction patterns for untreated and heat-treated quartz fibres.

Table 3
Density of untreated and heat-treated quartz fibres expressed as average value/standard deviation.

Temperature (°C)	Density (g/cm^3)
R.T.	2.218/0.043
600	2.212/0.019
700	2.209/0.015
800	2.243/0.029

leads to structural relaxation of internal deformation states, with anisotropy relaxation requiring shorter times and lower temperatures when compared to enthalpy relaxation. According to Feih [37], this phenomenon is consistent with a surface-controlled strength loss mechanism as structural relaxation occurs faster at the surface than in the bulk of the fibre. The presence of water arising from the decomposition of the silane-based sizing or absorbed to the glass surface has also been found to promote surface structural relaxation by attacking the silica network via thermally-activated stress-corrosion. As previously reported by Lilli et al. [20], this phenomenon can produce gradients of the mechanical properties across the cross-sectional area of heat-treated fibres. Therefore, to disclose possible structural heterogeneities and further investigate whether bulk changes are involved in the thermally-induced decay of quartz fibre strength, high-speed nano-indentation, and pillar-splitting experiments were employed for high-resolution mapping of the mechanical properties and fracture toughness assessment over the cross-section of fibres.

3.2. Mechanical characterization at the nanoscale

Fig. 8 and Fig. 9 report the nanoindentation elastic modulus and hardness data extracted from the high-speed mapping of representative fibre cross-sections as a function of the heat-treatment temperature. The high-resolution mechanical maps provide preliminary qualitative evidence of the absence of gradients in the mechanical response of the fibre across their cross-sectional area for all four treatment conditions studied. However, at the interface between the embedding matrix and the fibres, a steep gradient of both the elastic modulus and hardness is visible: an increment from the skin to core, which is generally attributable to artefacts caused by indents laying on both phases, determining a mixed mechanical response.

To further study and evidence possible differences in the nano-indentation response of the fibres, a comparison between quasi-static nanoindentations performed at the fibres centre and mechanical data obtained from averaging over central circular areas (4μm wide) extracted from each map has been performed (Fig. 10). Apart from discrepancies existing between values reported by CSM nanoindentation and high-speed mapping, arising from the intrinsic difference between the constant low-straining rate applied in one case and the higher (at least one order of magnitude greater) non-constant straining involved in the other, no statistically significant differences are reported for the fibres as a function of the treatment temperature, nor for the elastic modulus nor the hardness values for both quasi-static (Table 4) and high-speed mapping (Table 5). These analyses at the nanoscale confirm the macroscopic results obtained from single fibre tensile tests, whereas the different absolute values of Young's modulus have to be ascribed, also in this case, to the different nature of the two methods [20].

Probability Distribution Function (PDF) deconvolutions, able to identify a minimum of two different mechanical phases from elastic modulus and hardness response, were applied to the cross-sectional areas of the fibres to deeply understand the possible formation of gradients and quantify them in a statistically robust framework. As reported in supplementary material S1, no significant differences were revealed in the quartz response. While it is true that the PDF distributions are optimally reconstructed in all the cases with multi-variate bi-gaussian strategy (meaning that two phases are effectively present in the

mechanical response), the differences in values between the two and the corresponding standard error in their determination suggest that the two are most likely related to randomly distributed defects or local crystalline areas than a consistent microstructural gradient that could modify more than the 5% the two population of searched phases. Finally, Fig. 11 shows the k-means clustering analysis results, by which average and standard error values corresponding to the two mechanical phases are positionally identified within the fibre's cross-sectional area. It can be seen how no specific mechanical sub-structures are forming, while the thesis for which the clustered differences are due to randomly spatially distributed sub-surface features is enforced.

Before the drawing process, glass melts contain randomly oriented defects, like striae, microbubbles, and anisometric inhomogeneous domains, which are frozen-in in fibres during thermal quenching [17,47]. These defects are evidenced for quartz fibres by the randomly distributed clustered values of the elastic modulus and hardness over the fibre cross-section. This is still in line with the previous finding of a failure triggered by superficial flaws, although the observed bulk flaws may be considered potential fracture sources. The axial stress applied during the drawing process induces a preferential orientation of the defects along the fibre axis, considerably reducing the probability of initiating the fracture. The long-range preferential arrangement of flaws is unlikely to be relaxed by thermal exposure below the glass transition temperature, as a viscous state is required [17], making it reasonable to conclude that the bulk of the fibre is dotted with anisotropic flaws regardless of heat-treatment conditions.

To further investigate the effects of thermal exposure on the bulk properties of quartz fibres, the fracture toughness of untreated and heat-treated quartz fibres was evaluated through pillar-splitting experiments. Fig. 12 reports representative data for the Load versus Displacement-Into-Surface curves of micro-pillar splitting experiments performed to assess the fracture toughness of single quartz fibres at their centre, utilizing both CSM and high-speed mapping data, the latter, as described above, from selected areas corresponding to the fibre centre and having lateral dimensions equal to the diameter of the pillars. From this data, a reproducible and precise burst in the displacement could be seen for each population of fibres corresponding to the critical splitting event; its average value is seen to increase with the treatment temperature. Being the diameters equal and reproducible with each pillar and having reported no statistically relevant changes in the E/H response of the fibres with temperature (as well as within the cross-sectional area: see supplementary material S2), on which the calibration coefficient γ is dependent, this directly translates into an increase in the fracture toughness values from the non-treated case to the 800 °C treated fibres. Indeed, as evidenced in Fig. 13, a statistically significant increment in the K_c values exists between the latter two populations of $\sim$ 9% (Table 6).

In comparison, Feih et al. [11] found a unique K_c value for E-glass fibres, irrespective of heat-treatment temperature, while Lilli et al. [20] measured an increase in the K_c of heat-treated basalt fibres (up to 22% of its original value) by both single-edge notch tension (SENT) and pillar splitting techniques. In both studies, the possible variations in K_c are reported as evidence of the occurrence or not of bulk structural changes, being supported by other findings, such as possible changes in Young's modulus and density of the fibres and, in the case of Lilli's work, structural heterogeneities over the fibre cross-section. Interestingly, having reported no significant variations in the material-specific coefficient γ (related to the elastic–plastic properties), the here-measured increase in the fracture toughness is not dependent upon specific variations of the elastic and plastic response, being solely reliant on triggered modifications in the crack propagation resistance due to treatment.

Additional experiments have been performed to elucidate this trend as a function of the diametral position of the probed volume (micro-pillar). From testing of the population of micro-pillars machined at the edge of the fibre (for which the diametral dimensions have been reduced
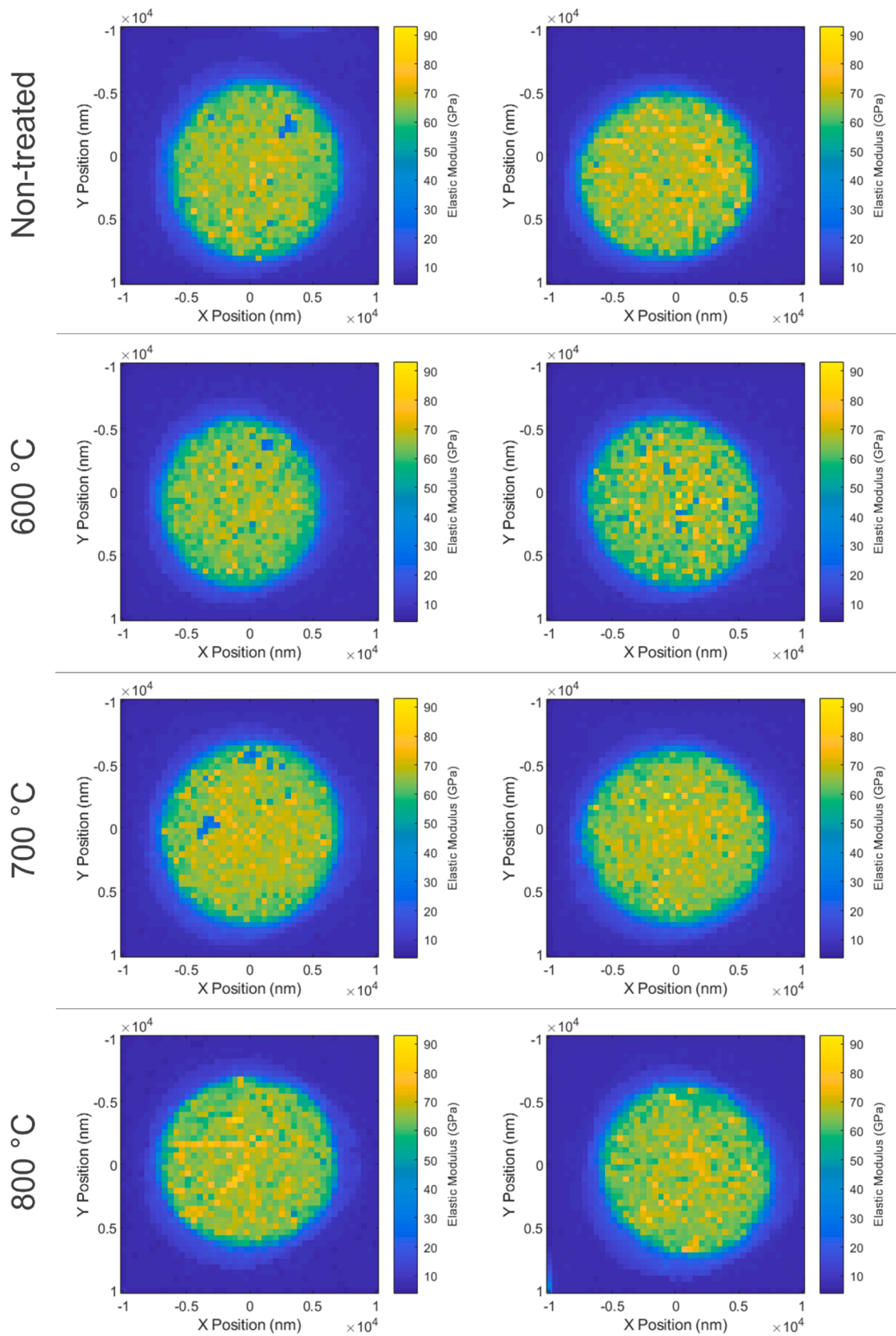
Fig. 8. Representative high-speed nanoindentation maps for the elastic modulus as a function of the heat-treatment temperature.
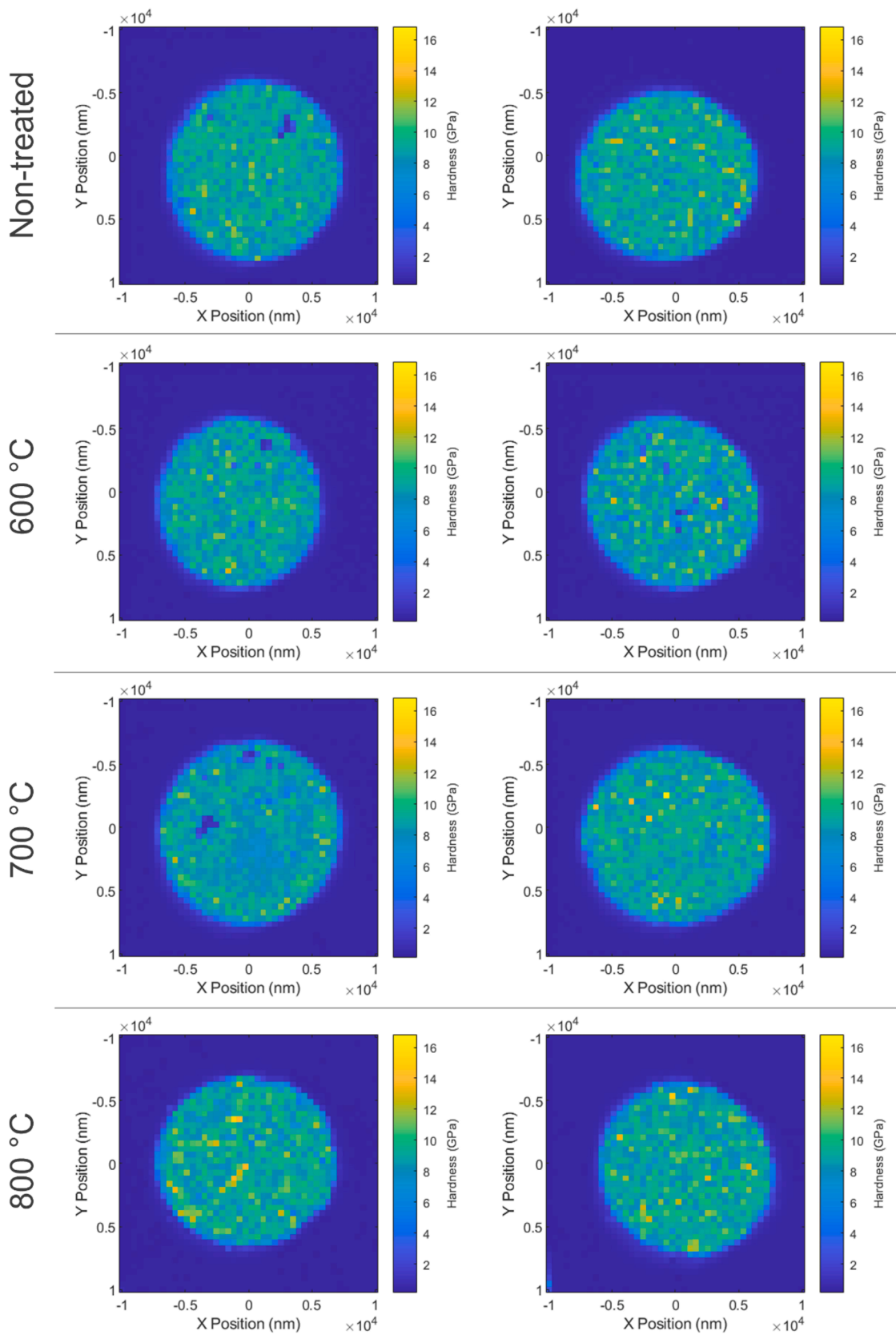
Fig. 9. Representative high-speed nanoindentation maps for the hardness as a function of the heat-treatment temperature.
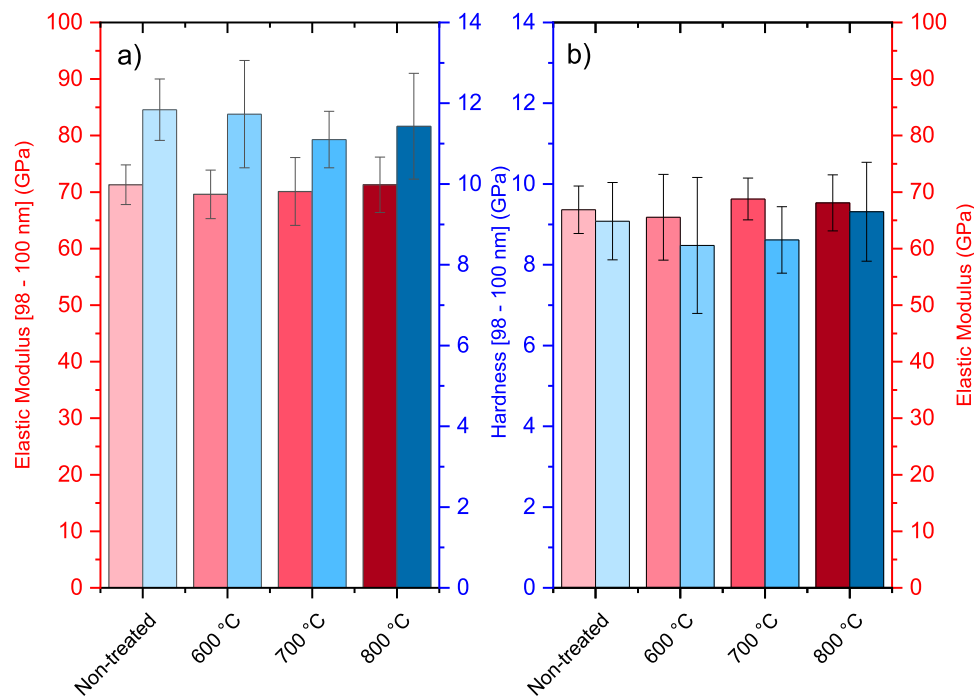
Fig. 10. Elastic modulus and Hardness values from nanoindentation experiments as calculated from a) Continuous Stiffness Measurements averaged across multiple tests over several fibres and b) data extrapolation from multiple high-speed maps at the fibre centre (in a lateral dimension whose position corresponds to the positioning of the pillars and their diameter).

Table 4
Mechanical properties of the quartz fibres as a function of the thermal treatment identified via Continuous Stiffness Nanoindentation experiments.

Sample	Elastic Modulus (GPa) [98–100 nm]	Hardness (GPa) [98–100 nm]	E/H
Non-treated	71.30 ± 3.50	11.84 ± 0.76	6.20 ± 0.48
600 °C	69.60 ± 4.30	11.73 ± 1.33	5.93 ± 0.76
700 °C	70.10 ± 6.00	11.1 ± 0.70	6.31 ± 0.67
800 °C	71.30 ± 4.90	11.43 ± 1.31	6.23 ± 0.83

Table 5
Mechanical properties of the quartz fibres as a function of the thermal treatment identified via data averaging high-speed nanoindentation maps over more than two fibres in areas corresponding to the positions of the pillars (fibres centre).

Sample	Elastic Modulus (GPa)	Hardness (GPa)	E/H
Non-treated	66.9 ± 4.2	9.1 ± 0.9	7.4 ± 0.9
600 °C	65.5 ± 7.6	8.5 ± 1.7	7.7 ± 1.7
700 °C	68.8 ± 3.7	8.6 ± 0.8	8.0 ± 0.9
800 °C	68.1 ± 4.9	9.3 ± 1.2	7.3 ± 1.1

with respect to those fabricated at the pillar centre to reduce the lateral size of each test and enhance the resolution), a similar trend is shown in Fig. 14, with an increase from the 700 °C treatment to the 800 °C treatment. While those values are not directly comparable with the ones from bigger diameters due to increasing positioning errors (as a function of the pillar diameter) and size effects when reducing the lateral size of a test, values are still compatible with the central position ones. This further confirms the previous finding, in which it was stated that the mechanical properties are not showing any specific gradient from the edge toward the centre of the fibre (being excluded those arising from mixed indentation responses as previously discussed).

The temperature-dependent evolution of fracture toughness suggests that quartz fibres are affected by exposure to temperatures between 600 and 800 °C. This effect occurs uniformly across the fibre cross-section without producing radial gradients. Although the nature of this phenomenon requires further investigation, it is important to note its relationship with the strength reduction. According to classic fracture mechanics theory, specifically to Griffith's formulations, a decrease in fibre strength may be attributed to a reduction in fracture toughness or an increase in flaw severity in size or shape. Therefore, increasing the crack propagation resistance should result in improved strength. Still, this phenomenon's extent is insufficient to offset the drastic effects that cause the strength to decrease significantly, which may arise from extrinsic critical-sized flaws.

Considering that, in pillar-splitting experiments, the critical size of the crack depends solely on its nucleation under the indenter tip and unstable propagation due to pillar-edge-dominated effects. The material-intrinsic growth in crack propagation resistance measured (intrinsic for the probed pillar volume) does not contradict the results of other investigations reported in this study. It is reasonable to assume that a mechanism causing strength degradation is mainly active at the surface of quartz fibres, which could involve the thermal-activated growth of pre-existing flaws or the development of new, more severe flaws.

4. Conclusions

The degradation of the tensile strength of quartz fibres following thermal exposure can limit their applications at high temperatures. In the present study, a strength loss up to 86% was detected after thermal conditioning in the temperature range 600–800 °C for 1 h in air. Mechanical characterizations at multiple length scales have been performed to investigate the possible damage mechanisms, focusing on understanding whether thermal exposure can affect the bulk properties of quartz fibres, i.e., Young's modulus, density, and fracture toughness, and the possible relationship with the strength decay. Compared to general-purpose glass fibres and basalt fibres [11–14,20,36,37], quartz fibres were found to exhibit a similar strength degradation behaviour, whereas their bulk properties appeared less sensitive to thermal exposure, being relatively stable after heat treatment up to 800 °C. No bulk
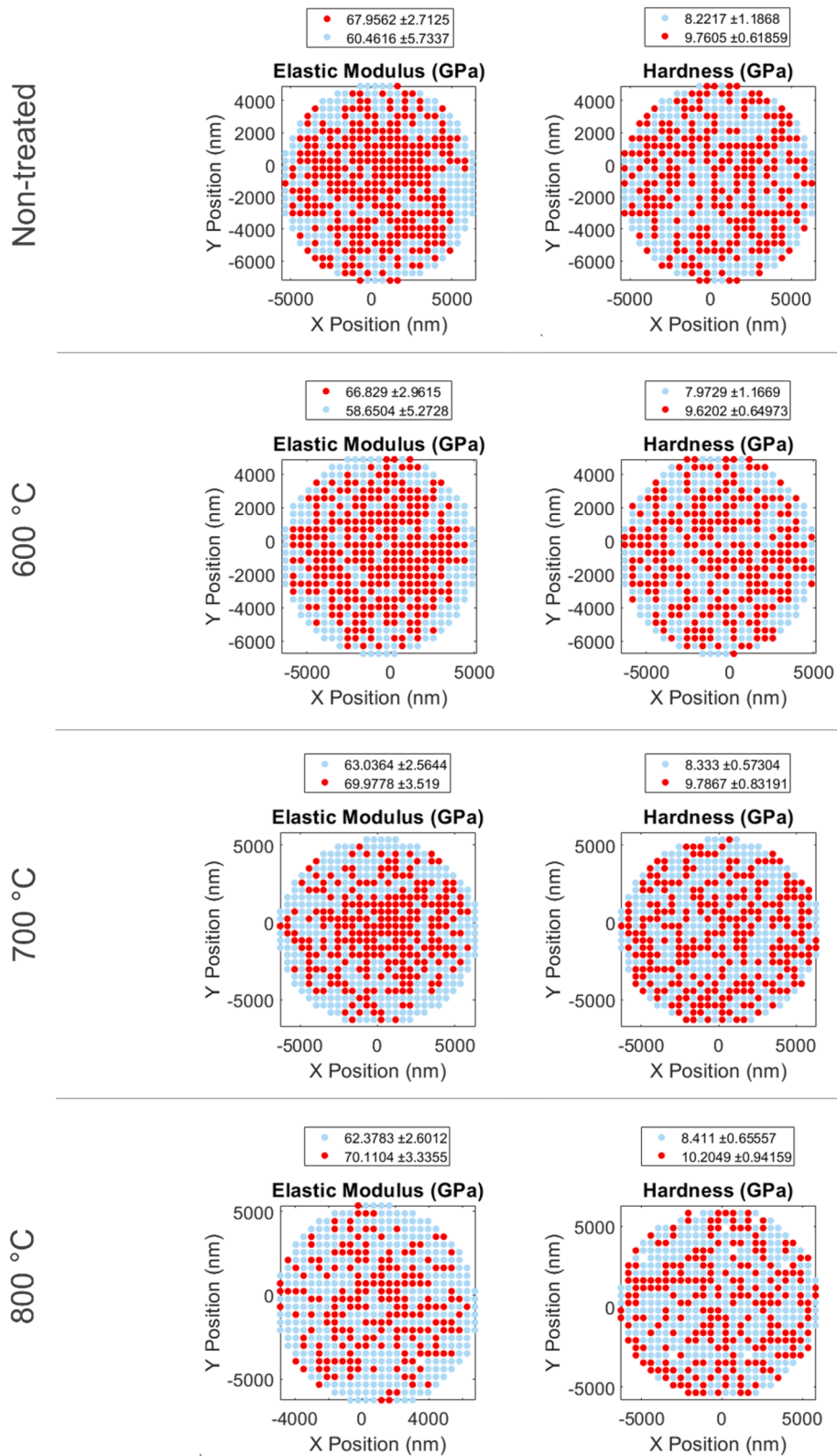
Fig. 11. K-means clustering to study secondary phases (two targeted clusters) distributions within the fibres compared with PDF deconvolution data from supplementary material S1.

crystallization phenomena or statistically significant differences in Young's modulus and hardness values were detected.

Interestingly, a 9% increase in the fracture toughness revealed an enhanced resistance to crack propagation following heat treatment suggesting that, albeit limited, quartz fibres experienced a bulk modification effect which will be the topic of further research. The thermal-induced strength decay of quartz fibres was ascribed to surface-controlled mechanisms involving the exposure and growth of inherent flaws and possible development of new, more severe, defects whose negative effect on the tensile strength cannot be compensated by the
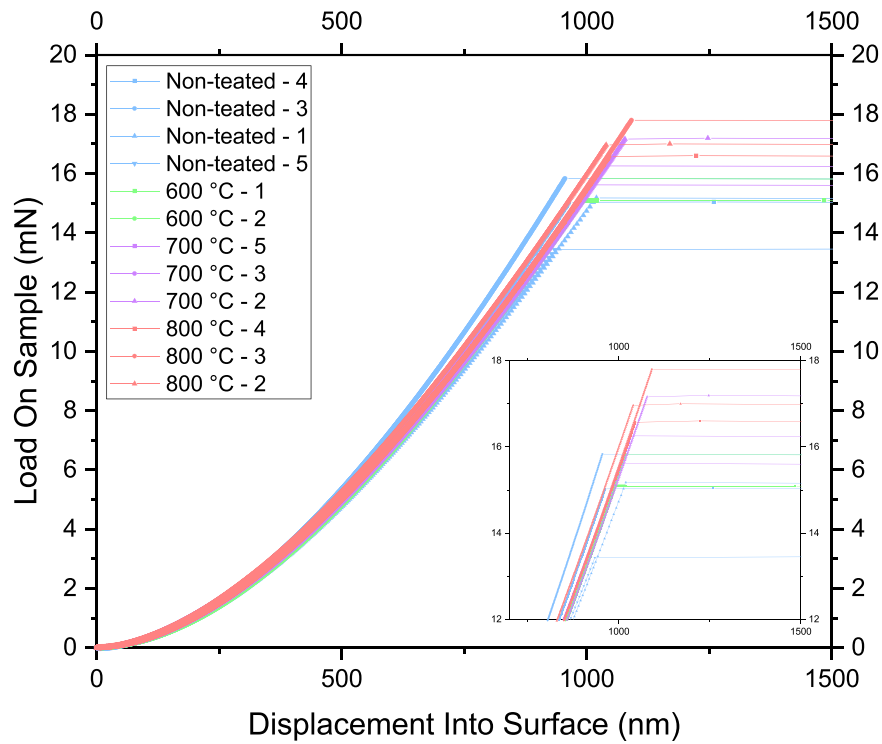
Fig. 12. Load On Sample versus Displacement Into Surface curves corresponding to representative micro-pillar splitting experiments performed on the fibres samples. The inset magnifies differences into the pop-in event corresponding to pillar-splitting for each heat-treated population.
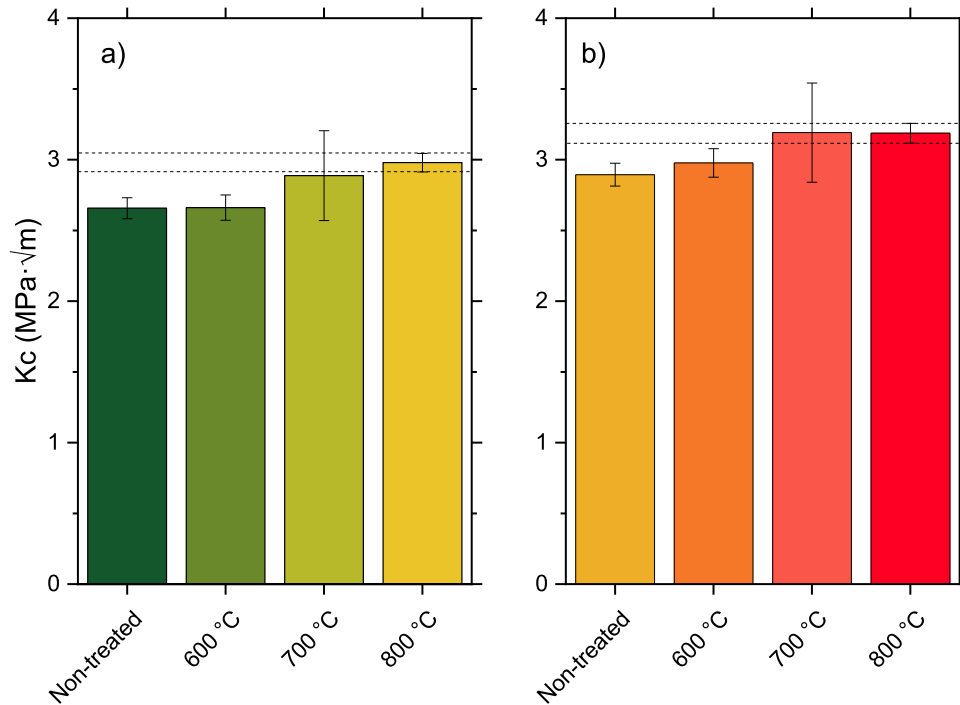

Fig. 13. Fracture toughness as a function of the thermal treatment obtained from micro-pillar splitting experiments. Comparison between values of the γ coefficient as obtained from a) continuous stiffness measurements at the centre of the fibres and b) values obtained from high-speed data points corresponding to pillar positions at the fibre centre.

slightly improved crack propagation resistance. Mechanical handling damage, localized crystallization, relaxation of structural anisotropy and water attacking, all acting at the surface of quartz fibres, are considered possible damage mechanisms, requiring future investigations to be verified. The outcomes of this study can be used to design solutions to prevent the thermal strength loss of quartz fibres. For instance, applying high-temperature resistant coatings [5,7,10] on quartz fibre surface and other surface modification strategies might be effective ways to reduce their susceptibility to surface degradation and, thus, strength reduction after thermal exposure.

Table 6

Critical loads (P_c), calibration coefficients and fracture toughness values as calculated from experiments at the centre of the fibres from two evaluation procedures for the mechanical properties (i.e., Continuous Stiffness Measurements and High-speed nanoindentation mapping).

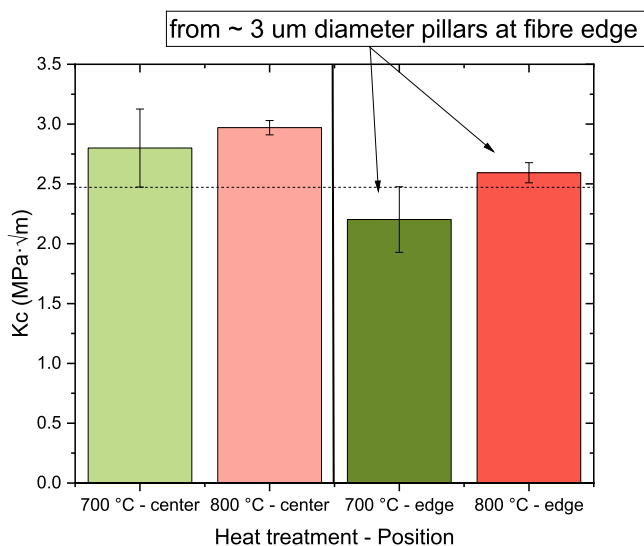| Sample	P_c	γ (CSM)	γ (High-speed)	K_c $(MPa\sqrt{m})$ CSM	K_c $(MPa\sqrt{m})$ High-speed
Non-treated	14.87 ± 4.19	0.501745	0.546467	2.65 ± 0.07	2.89 ± 0.08
600 °C	15.46 ± 0.52	0.498667	0.557899	2.66 ± 0.89	2.97 ± 0.10
700 °C	16.34 ± 0.77	0.511834	0.565716	2.88 ± 0.31	3.19 ± 0.35
800 °C	16.95 ± 0.37	0.509192	0.544761	2.97 ± 0.06	3.18 ± 0.06

Fig. 14. Fracture toughness trends at the fibre edge were reported compared with values from bigger pillars fabricated at the centre. The rising trend of fracture toughness with treatment temperature is consistent also for the edge of the fibres, while lower values compared to 4 μm diameter pillars depend upon increasing positioning error for lower diameters and size effects.

Declaration of Competing Interest

The authors declare that they have no known competing financial interests or personal relationships that could have appeared to influence the work reported in this paper.

Acknowledgements

Appendix A. Supporting information

Supplementary data associated with this article can be found in the online version at doi:10.1016/j.jeurceramsoc.2023.07.048.

References

[1] L. Tang, J. Zhang, Y. Tang, J. Kong, T. Liu, J. Gu, Polymer matrix wave-transparent composites: a review, J. Mater. Sci. Technol. vol. 75 (2021) 225–251, https://doi.org/10.1016/j.jmst.2020.09.017.

[2] J. Zhang, Z. Liu, M. Han, J. Zhang, Y. Tang, J. Gu, Block copolymer functionalized quartz fibers/cyanate ester wave-transparent laminated composites, J. Mater. Sci. Technol. vol. 139 (2023) 189–197, https://doi.org/10.1016/j.jmst.2022.09.005.

[3] L.A. Rodriguez, C. García, L.R. Grace, The effect of in-service aerospace contaminants on X-band dielectric properties of a bismaleimide/quartz composite, AIP Conf. Proc. vol. 1664 (2015), https://doi.org/10.1063/1.4918423.

[4] S. Anirudh, C.G. Jayalakshmi, A.A. Mokhtar, A. Anand, B. Kandasubramanian, Effect of repeated thermal cycle on compressive properties of cyanate ester/quartz-based composites, Mater. Today Proc. vol. 62 (2022) 5292–5297, https://doi.org/10.1016/j.matpr.2022.03.365.

[5] Y. Zheng, S. Wang, The effect of SiO 2 -doped boron nitride multiple coatings on mechanical properties of quartz fibers, Appl. Surf. Sci. vol. 258 (7) (2012) 2901–2905, https://doi.org/10.1016/j.apsusc.2011.11.004.

[6] A. Kulesh, M. Eronyan, I. Meshkovskii, V. Zolotarev, M. Bisyarin, M. Tsibinogina, Crystallization of quartz glass fibers during the drawing process, Cryst. Growth Des. vol. 15 (6) (2015) 2831–2834, https://doi.org/10.1021/acs.cgd.5b00253.

[7] H.R. Lu, C.A. Wang, Fabrication and characterization of ceramic coatings with alumina-silica sol-incorporated α-alumina powder coated on woven quartz fiber fabrics, Ceram. Int. vol. 39 (6) (2013) 6041–6050, https://doi.org/10.1016/j.ceramint.2013.01.020.

[8] Q.H. Wei, C.H. Wang, H.S. Wang, L. Li, Q. Luan, R. Liao, B. Dong, Disposing of silica fiber' surface, Key Eng. Mater. vol. 512 (2012) 559–562, https://doi.org/10.4028/www.scientific.net/KEM.512-515.559.

[9] Q.H. Wei, C.H. Wang, Z.Q. Cheng, L. Li, H.S. Wang, Z.H. Wei, F. Gao, Effects of different heat treatment temperatures on the properties of quartz fibers, Adv. Mater. Res. vol. 105 (2010) 115–118, https://doi.org/10.4028/www.scientific.net/AMR.105-106.115.

[10] L. Wang, Y.D. Huang, L. Liu, J.B. Zhang, The influence of PBO coating on room temperature mechanic properties of heat-treated quartz fiber-reinforced methyl silicon resin composites. I. Flexural properties, Mater. Sci. Eng. A vol. 465 (1–2) (2007) 22–28, https://doi.org/10.1016/j.msea.2007.04.036.

[11] S. Feih, A.P. Mouritz, S.W. Case, Determining the mechanism controlling glass fibre strength loss during thermal recycling of waste composites, Compos. Part A Appl. Sci. Manuf. vol. 76 (2015) 255–261, https://doi.org/10.1016/j.compositesa.2015.06.006.

[12] J.L. Thomason, L. Yang, R. Meier, The properties of glass fibres after conditioning at composite recycling temperatures, Compos. Part A Appl. Sci. Manuf. vol. 61 (2014) 201–208, https://doi.org/10.1016/j.compositesa.2014.03.001.

[13] P. Jenkins, S. Riopedre-Méndez, E. Sáez-Rodríguez, L. Yang, and J.L. Thomason, "Investigation of the strength of thermally conditioned basalt and E-glass fibres," in: 20th International Conference on Composite Materials, 2015.

[14] F. Sarasini, J. Tirillò, M.C. Seghini, Influence of thermal conditioning on tensile behaviour of single basalt fibres, Compos. Part B Eng. vol. 132 (2018) 77–86, https://doi.org/10.1016/j.compositesb.2017.08.014.

[15] L. Yang, J.L. Thomason, Effect of silane coupling agent on mechanical performance of glass fibre, J. Mater. Sci. vol. 48 (5) (2013) 1947–1954, https://doi.org/10.1007/s10853-012-6960-7.

[16] K.M. Davis, M. Tomozawa, Water diffusion into silica glass: structural changes in silica glass and their effect on water solubility and diffusivity, J. Non Cryst. Solids vol. 185 (3) (1995) 203–220, https://doi.org/10.1016/0022-3093(95)00015-1.

[17] M.D. Lund, Y. Yue, Impact of drawing stress on the tensile strength of oxide glass fibers, J. Am. Ceram. Soc. vol. 93 (10) (2010) 3236–3243, https://doi.org/10.1111/j.1551-2916.2010.03879.x.

[18] L. Yang, J.L. Thomason, The thermal behaviour of glass fibre investigated by thermomechanical analysis, J. Mater. Sci. vol. 48 (2013) 5768–5775, https://doi.org/10.1007/s10853-013-7369-7.

[19] W.H. Otto, Compaction effects in glass fibers, J. Am. Ceram. Soc. vol. 44 (2) (1961) 68–72, https://doi.org/10.1111/j.1151-2916.1961.tb15352.x.

[20] M. Lilli, E. Rossi, J. Tirillò, F. Sarasini, L. Di Fausto, T. Valente, C. González, A. Fernández, C. Lopes, R. Moscatelli, E. Bemporad, M. Sebastiani, Quantitative multi-scale characterization of single basalt fibres: insights into strength loss mechanisms after thermal conditioning, Mater. Sci. Eng. A vol. 797 (2020), 139963, https://doi.org/10.1016/j.msea.2020.139963.

[21] Y. Zheng, S. Wang, Effect of moderately high temperature heat treatment on surface morphology and structure of quartz fibers, Appl. Surf. Sci. vol. 258 (10) (2012) 4698–4701, https://doi.org/10.1016/j.apsusc.2012.01.062.

[22] M. Sebastiani, K.E. Johanns, E.G. Herbert, F. Carassiti, G.M. Pharr, A novel pillar indentation splitting test for measuring fracture toughness of thin ceramic coatings,

Philos. Mag. vol. 95 (16–18) (2015) 1928–1944, https://doi.org/10.1080/14786435.2014.913110.

[23] M. Sebastiani, K.E. Johanns, E.G. Herbert, G.M. Pharr, Measurement of fracture toughness by nanoindentation methods: recent advances and future challenges, Curr. Opin. Solid State Mater. Sci. vol. 19 (6) (2015) 324–333, https://doi.org/10.1016/j.cossms.2015.04.003.

[24] G. Bolelli, M.G. Righi, M.Z. Mughal, R. Moscatelli, O. Ligabue, N. Antolotti, M. Sebastiani, L. Lusvarghi, E. Bemporad, Damage progression in thermal barrier coating systems during thermal cycling: a nano-mechanical assessment, Mater. Des. vol. 166 (2019), 107615, https://doi.org/10.1016/j.matdes.2019.107615.

[25] T. Beirau, E. Rossi, M. Sebastiani, W.C. Oliver, H. Pöllmann, R.C. Ewing, Fracture toughness of radiation-damaged zircon studied by nanoindentation pillar-splitting, Appl. Phys. Lett. vol. 119 (23) (2021), 231903, https://doi.org/10.1063/5.0070597.

[26] ASTM, C1557: standard test method for tensile strength and young ' s modulus of fibers, Annu. B. ASTM Stand. vol. 03 (Reapproved 2013) (2014) 1–10.

[27] J.D. Sullivan, P.H. Lauzon, Experimental probability estimators for Weibull plots, J. Mater. Sci. Lett. vol. 5 (12) (1986) 1245–1247, https://doi.org/10.1007/BF01729379.

[28] M. Sebastiani, R. Moscatelli, F. Ridi, P. Baglioni, F. Carassiti, High-resolution high-speed nanoindentation mapping of cement pastes: Unravelling the effect of microstructure on the mechanical properties of hydrated phases, Mater. Des. vol. 97 (2016) 372–380, https://doi.org/10.1016/j.matdes.2016.02.087.

[29] E.P. Koumoulos, S.A.M. Tofail, C. Silien, D. De Felicis, R. Moscatelli, D. A. Dragatogiannis, E. Bemporad, M. Sebastiani, C.A. Charitidis, Metrology and nano-mechanical tests for nano-manufacturing and nano-bio interface: challenges & future perspectives, Mater. Des. vol. 137 (2018) 446–462, https://doi.org/10.1016/j.matdes.2017.10.035.

[30] B. Vignesh, W.C. Oliver, G.S. Kumar, P.S. Phani, Critical assessment of high speed nanoindentation mapping technique and data deconvolution on thermal barrier coatings, Mater. Des. vol. 181 (2019), 108084, https://doi.org/10.1016/j.matdes.2019.108084.

[31] P.S. Phani, W.C. Oliver, A critical assessment of the effect of indentation spacing on the measurement of hardness and modulus using instrumented indentation testing, Mater. Des. vol. 164 (2019), 107563, https://doi.org/10.1016/j.matdes.2018.107563.

[32] G. Constantinides, K.S. Ravi Chandran, F.J. Ulm, K.J. Van Vliet, Grid indentation analysis of composite microstructure and mechanics: Principles and validation, Mater. Sci. Eng. A vol. 430 (1–2) (2006) 189–202, https://doi.org/10.1016/j.msea.2006.05.125.

[33] F.J. Ulm, M. Vandamme, C. Bobko, J. Alberto Ortega, K. Tai, C. Ortiz, Statistical indentation techniques for hydrated nanocomposites: concrete, bone, and shale, J. Am. Ceram. Soc. vol. 90 (9) (2007) 2677–2692, https://doi.org/10.1111/j.1551-2916.2007.02012.x.

[34] M. Ghidelli, M. Sebastiani, K.E. Johanns, G.M. Pharr, Effects of indenter angle on micro-scale fracture toughness measurement by pillar splitting, J. Am. Ceram. Soc. vol. 100 (12) (2017) 5731–5738, https://doi.org/10.1111/jace.15093.

[35] M.H. Berger, D. Jeulin, Statistical analysis of the failure stresses of ceramic fibres: dependence of the Weibull parameters on the gauge length, diameter variation and fluctuation of defect density, J. Mater. Sci. vol. 38 (2003) 2913–2923, https://doi.org/10.1023/A:1024405123420.

[36] P.G. Jenkins, L. Yang, J.J. Liggat, J.L. Thomason, Investigation of the strength loss of glass fibre after thermal conditioning, J. Mater. Sci. vol. 50 (3) (2015) 1050–1057, https://doi.org/10.1007/s10853-014-8661-x.

[37] S. Feih, E. Boiocchi, G. Mathys, Z. Mathys, A.G. Gibson, A.P. Mouritz, Mechanical properties of thermally-treated and recycled glass fibres, Compos. Part B Eng. vol. 42 (3) (2011) 350–358, https://doi.org/10.1016/j.compositesb.2010.12.020.

[38] H.G. De Luca, D.B. Anthony, E.S. Greenhalgh, A. Bismarck, M.S.P. Shaffer, Piezoresistive structural composites reinforced by carbon nanotube-grafted quartz fibres, Compos. Sci. Technol. vol. 198 (2020), 108275, https://doi.org/10.1016/j.compscitech.2020.108275.

[39] P. Zinck, M.F. Pay, R. Rezakhanlou, J.F. Gerard, Mechanical characterisation of glass fibres as an indirect analysis of the effect of surface treatment, J. Mater. Sci. vol. 34 (1999) 2121–2133, https://doi.org/10.1023/A:1004572112470.

[40] R. Danzer, A general strength distribution function for brittle materials, J. Eur. Ceram. Soc. vol. 10 (6) (1992) 461–472, https://doi.org/10.1016/0955-2219(92)90021-5.

[41] S. Feih, K. Manatpon, Z. Mathys, A.G. Gibson, A.P. Mouritz, Strength degradation of glass fibers at high temperatures, J. Mater. Sci. vol. 44 (2) (2009) 392–400, https://doi.org/10.1007/s10853-008-3140-x.

[42] S. Feih, A. Thraner, H. Lilholt, Tensile strength and fracture surface characterisation of sized and unsized glass fibers, J. Mater. Sci. vol. 40 (2005) 1615–1623, https://doi.org/10.1007/s10853-005-0661-4.

[43] P.G. Jenkins, L. Yang, J.L. Thomason, X. Chen, J.F. Watts, S.J. Hinder, Investigation of chemical and physical surface changes of thermally conditioned glass fibres, Fibers vol. 7 (1) (2019) 7, https://doi.org/10.3390/fib7010007.

[44] M.D. Lund, Y. Yue, Fractography and tensile strength of glass wool fibres, " J. Ceram. Soc. Jpn. vol. 116 (1356) (2008) 841–845, https://doi.org/10.2109/jcersj2.116.841.

[45] F. Islam, S. Joannès, L. Laiarinandrasana, Evaluation of critical parameters in tensile strength measurement of single fibres, J. Compos. Sci. vol. 3 (3) (2019) 69, https://doi.org/10.3390/jcs3030069.

[46] J.L. Thomason, U. Nagel, L. Yang, D. Bryce, A study of the thermal degradation of glass fibre sizings at composite processing temperatures, Compos. Part A Appl. Sci. Manuf. vol. 121 (2019) 56–63, https://doi.org/10.1016/j.compositesa.2019.03.013.

[47] J. Murach and R. Briickner, Preparation and structure-sensitive investigations on silica glass fibers, vol. 211, no. 3, pp. 250–261, 1997, doi:https://doi.org/10.1016/S0022–3093(96)00635–7.